Journal of Materials Chemistry A

Accepted Manuscript

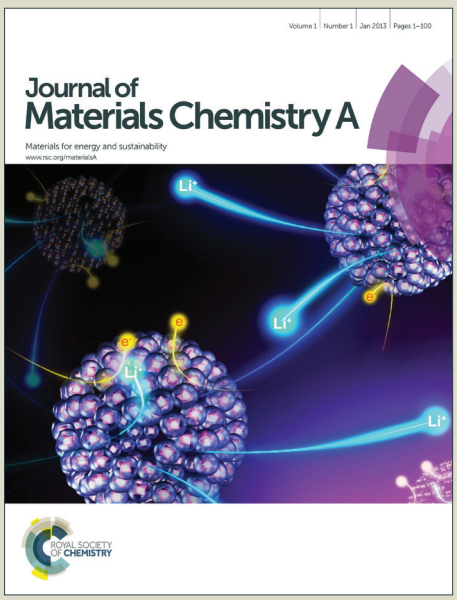

ROYAL SOCIETY OF CHEMISTRY

www.rsc.org/materialsA

Decoupled ion conduction in poly(2-acrylamido 2methyl-1-propane-sulfonic acid) homopolymers

Siti Aminah Mohd Noor,[a,b] Jiazeng Sun,[a] Douglas R MacFarlane[a,c] , M. Armand[d], D. Gunzelmann[e] and Maria Forsyth,[c,e]

[a] *School of Chemistry, Monash University, Clayton Campus, Victoria, Australia*

[b] *Chemistry Department, Centre for Defence Foundation Studies, National Defence University of Malaysia, 57000, Kuala Lumpur, Malaysia*

[c] *ARC Centre of Excellence for Electromaterials Science (ACES)*

d CIC Energigune, Vitoria, Spain

[e] *Institute for Frontier Materials Deakin University, Victoria, Australia*

[*]aminah.mohd.noor@monash.edu; *mforsyth@deakin.edu.au*

ABSTRACT

As the focus on developing new polymer electrolytes continues to intensify in the area of alternative energy conversion and storage devices, the rational design of polyelectrolytes with high single ion transport rates has emerged as a primary strategy for enhancing device performance. Previously, we reported a series of sulfonate based copolymer ionomers based on using mixed bulky quaternary ammonium cations and sodium cations as the ionomer counterions. This led to improvements in the ionic conductivity and an apparent decoupling from the T_g of the ionomer. In this article, we have prepared a new series of ionomers based on the homopolymer of poly(2-acrylamido 2methyl-1-propane-sulfonic acid) using differing sizes of the ammonium counter-cations. We observe a decreasing T_g with increasing the bulkiness of the quaternary ammonium cation, and an increasing degree of decoupling from T_g within these systems. Somewhat surprisingly, phase separation is observed in this homopolymer system, as evidenced from

multiple impedance arcs, Raman mapping and SEM. The thermal properties, morphology and the effect of plasticizer on the transport properties in these ionomers are also presented. The addition of 10 wt.% plasticizer increased the ionic conductivity between two and three orders of magnitudes leading to materials that may have applications in sodium based devices.

Keywords: single ion conductor, ionomer, conductivity, sodium ion, decoupling

INTRODUCTION

The electrolyte is a key component of an electrochemical device, since it serves as the medium for ionic transport, and thus much research has been expended on improving the performance, safety and cost of electrolytes[1-5]. One way to improve the safety of a device, such as a battery, is to develop a solid state electrolyte with appropriate target ion transport properties. In this respect, solid polymer electrolytes (SPEs) have been investigated since the late 1970s[6]. The use of a SPE in a power source leads to improvements in performance by providing mechanical stability (flexibility and moldability), reduced weight, and operational safety (no leakage of corrosive materials and zero volatility/flammability)[4, 7-9].

SPEs based on polyethers have been extensively studied for applications in Lithium batteries[10-12], however, their performance is limited by the fact that the cation transport number (eg. Li^+) is significantly less than 0.5 and thus anion aggregation occurs at the electrode interface; this eventually leads to concentration polarization of the electrode[13-16]. To overcome this polarization, one needs to ensure that the

cation transport number is as close to unity as possible. One way to do this is to tether the anionic species covalently to the polymer backbone or an attached pendant group[10, 17-19]. This allows the counter-cation to be the sole charge carrier. Such polyelectrolyte systems are often referred to as ionomers. Kobayashi et al.[20] reported that the lithium transport number of P(MEO-MALi) polymer electrolyte system is unity, as the carboxylate anions of this system were covalently bonded to the polymer chains. Sodium ion as single ion conductor in ionomer system also has been investigated in the system of poly(sodium 2-[ω-metharyloyloligo(oxyethylene)] ethylsulfonate) by Zheng et al.[21] In this system, the short oligo(oxyethylene) chains facilitate the dissociation of sodium sulfonate and the flexible macromolecular chains promote the transfer of the Na^+ ions.

Other single-ion conducting ionomers systems have been developed[10, 20-24]; yet these systems display ionic conductivities far lower than their polymer/salt mixture counterparts. Various techniques have been employed to increase the ionic conductivity of these materials, such as incorporation of an organic solvent or ionic liquid[10, 12, 25, 26] to assist the cation dissociation from the polymer backbone. Even though these materials provide high ionic conductivity as well as good elastomeric properties, the existence of a low molecular weight solvent leaves the possibility that the electrolytes may leak or be volatile.

Very recently, we reported the development of solvent free solid ionomer electrolytes based on the copolymer poly([triethylmethylammonium][2-acrylamido-2-methyl-1-propane-sulfonic acid]-co-sodium[vinyl sulfonate], poly([N_{1222}][AMPS]-co-Na[VS]), where a fraction of sodium ions were replaced

with a bulky quaternary ammonium cation[19]. This is designed to create anion centers on the polymer that are less associated with a cation and therefore that the metal cation motion may be less coupled to the bulk dynamics of the ionomer. We found that significant ionic conductivity was measurable below T_g in these systems, indicating an increasingly decoupled ion transport mechanism from the ionomer's backbone motions and structural relaxations (which are responsible for the glass transition temperature, T_g) as the ratio of the sodium to quaternary ammonium cation decreased.

This remarkable finding has prompted us to study the effect of different types of ammonium cation on the conductivity of ionomers and also to investigate the differences between homopolymer ionomer and copolymer ionomer systems. In this work, we prepare three different ammonium-based homopolymer ionomers (where the alkyl chain length on the counterion is modified) and also a series of ionomers containing the triethylmethylammonium (N_{1222}) cation and different amounts of Na^+ (poly(N_{xyyy})$_z$$Na_{1-z}$[AMPS]). This system can be compared with the copolymer ionomer system previously reported by us. These samples are characterized using DSC to determine the glass transition and a.c. impedance spectroscopy to measure ionic conductivity, while solid state NMR was performed to study the dynamic behavior of the ionomers. Raman Spectroscopy and SEM have also been used to observe the ionomer's morphology.

EXPERIMENTAL

Sample preparation

Preparation of poly(2-acrylamido-2-methyl-1-propane-sulfonic acid) (PAMPS) (alkyl-ammonium/sodium salts) was carried out based on Scheme 1. Typical procedures for synthesis of a PAMPS sample are as follows: 5.017 g of AMPS (0.0241 mol, Aldrich) were dissolved in 10ml of distilled water; to form the sodium salt, NaOH-water solution containing 0.01205 mol of NaOH was added drop-wise at room temperature with magnetic stirring until the pH value of the solution reached ~7. In the same way a certain amount of the tetraalkyl ammonium-carbonate solution (Aldrich) was added to the AMPS solution to form the tetraalkyl ammonium salt. ~0.2% (w/w) $K_2S_2O_8$ was then added and the solution was stirred at ~85 °C for 2 days. After removing the solvents from the polymer/homopolymer solutions all the prepared samples were dried under vacuum at ~70 °C for at least 2 days before any characterisation was undertaken. Two types of plasticizer have been used in this system; these are tetraglyme (tetraethylene glycol dimethyl ether (purum, ≥99.0% (GC), Fluka)) and N,N-dimethyl-3-methoxypropylammonium bis(trifluoromethylsulfonyl)imide ($N_{22(3O1)2}$TFSI) which was prepared as reported elsewhere[27-29]. The ionic conductivity of $N_{22(3O1)2}$TFSI at room temperature was 1.9 x 10^{-3} S.cm^{-1}

Scheme 1

Ionic Conductivity

The ionic conductivity of the ionomers was measured by ac impedance spectroscopy using a high frequency response analyzer (HFRA; Solartron 1296). The powder samples were first pressed into pellets (1 mm thick and 13 mm in diameter) using a

KBr die and a hydraulic press at 10 tonne for 30 min; pellets were pressed and aged in the oven at 443 K overnight; pressed pellets were coated with gold using a gold sputter coater (SPI-Module Sputter Coater - Division of Structure Probe Inc. with plasma uses argon gas) at plasma current of about 20 mA (DC) for 2 minutes and then sandwiched between two stainless steel blocking electrodes. Data was collected over a frequency range of 0.1 Hz to 10 MHz (ten points per decade) with a 30 mV amplitude over a temperature range of 363 to 443 K in 10 K intervals. The temperature was controlled to within 1 K using a Eurotherm 2204e temperature controller and a band heater with a cavity for the cell using a thermocouple type T, which was embedded in the cell. The sample was held for a short equilibration time, up to 2 minutes, to stabilize the temperature prior to impedance measurement. The conductance was determined from the impedance data using the series circuit in Z-view (Version 2.3), see Supplementary Information for further details. Conductivity data plotted is the mean and standard error of repeated heating and cooling runs in each case

Differential Scanning Calorimetry (DSC)

DSC measurements were carried out on the as-prepared samples, using a DSC Q100 series instrument (TA Instruments), and the data was evaluated with Universal Analysis 2000 software. Approximately 8 to 10 mg of the ionomer sample was hermetically sealed in Aluminium pans and measured over a temperature range of 273 to 423 K at a scanning rate of 10 $K.min^{-1}$. The glass transition temperature was determined from the onset of the heat-capacity change during the heating ramp.

Solid-state nuclear magnetic resonance (NMR)

Solid-State NMR spectra were recorded with a BRUKER Avance III 300WB spectrometer operating at 300.13, 79.39, 125.76 and 30.42 MHz for ^{1}H, ^{23}Na, ^{13}C and ^{15}N, respectively. All ^{1}H and ^{13}C spectra are given relative to tetramethylsilane, ^{15}N spectra with respect to nitromethane and ^{23}Na spectra were referenced to 1M $NaCl_{(aq)}$. Samples were packed in standard 4mm MAS rotors, loaded and measured in a 4 mm double-resonance MAS probe (BRUKER) spinning at 10 kHz. Cross-Polarization from ^{1}H was used to excited ^{13}C and ^{15}N nuclei applying a ramped (50 to 100% power) shape pulse on the proton frequency with a contact time of 2 and 10 ms, respectively. A SPINAL64 high power proton decoupling with a nutation frequency of 114 kHz was applied during acquisition. Recycle delays were set between 3-5 times the proton T_1 relaxation constants, which were determined earlier. Static ^{1}H and ^{23}Na spectra were measured with a solid-echo sequence using a 2.5 μs, 90 degree pulse and an echo delay of 20 μs.

Raman Spectroscopy

For Raman mapping measurements, a confocal Raman system, Witec 300R, based on an integral Olympus BX40 microscope with a 50x objective (8 mm) was used. The spatial resolution was about 2 μm. The calibration was undertaken referring to the 520.5 cm^{-1} line of silicon. A 785 nm laser source was used for excitation. The collection time for each spectrum was 1 s with one accumulation. The spectrometer grating had 80 points/line. An automatic motorized translator X – Y stage was used to perform Raman mapping.

Raman images were recorded by first positioning the ionomer sample in the laser focus using a video camera and white-light illumination, followed by scanning over the mapping region (selected as 250 x 250 μm^2 in step sizes of 3 μm) and accumulating a full spectrum at each pixel. A total of 6400 Raman spectra (250 x 250 probe spots) were measured for each sample. Witec Project processing software was used to operate the mapping system, record the spectra and process the data.

Scanning Electron Microscopy (SEM)

SEM images were collected using a Phillips XL20 SEM with an Oxford X-Max 50 mm^2 silicon drift detector. The accelerating voltage used was 5k

RESULTS AND DISCUSSION

1. Effect of ammonium cation alkyl chain length in the homopolymer of (poly(N_{xyyy})$_{0.5}$$Na_{0.5}$[AMPS])

Thermal properties

Fig. 1 shows the DSC thermograms of the sodium homopolymer systems at a cation ratio of 50:50 (poly(N_{xyyy})$_{0.5}$$Na_{0.5}$[AMPS]) , with three different quaternary ammonium cations. It can be seen that N_{1444}^+ containing system has a lower T_g compared to the N_{1222}^+ system. This is expected since the aliphatic chains in N_{1444}^+ are bigger and bulkier than the ethyl groups on the N_{1222}^+ cation, which lead to lower inter- and intra-chain ionic interactions. Although it is well known that T_g increases with ion content due to the presence of physical cross-links, this effect is notably reduced with larger counterions[30,31, 32]. Tudyryn et al. reported that[31], with constant ion content, their polyester-sulfonate ionomers showed T_g decreasing as counterion size increases. They suggest that this is caused by two factors[32, 33] (i) larger

counterions associate less with the backbone anions, forming fewer and weaker physical cross-links that then leads to a decrease in T_g for ionomers (ii) larger counterions act as plasticizers, further lowering T_g.

However, $N_{14,111}^+$ possesses the highest T_g, among the ionomers prepared in this work, despite having the longest aliphatic chain. This may be due to there only being one long aliphatic chain on the nitrogen atom along with the three methyl groups, which makes the cation effectively less bulky compared to N_{1444}^+ and thus the charge on the nitrogen in the $N_{14,111}^+$ cation may be less sterically shielded, leading to stronger ionic interaction with the polymer anionic groups. This finding is similar to the behavior reported by Weiss et al.[34] where they investigated ionic interactions in sulfonated polystyrene ionomers by use of alkyl-substituted ammonium counterions. They found that the relative degree of ionic interaction in their materials can be summarized as follows: $NH_4^+ > BuNH_3^+ > Me_3NH^+ > Bu_2NH_2^+ \sim Bu_4N^+ > Bu_3NH^+ \sim PS$, where Bu = C_4H_9 and Me = CH_3. The ionic interaction of $BuNH_3$ is stronger than Me_3NH even though the alkyl chain in $BuNH_3$ is longer. They also suggested that more significant decreases in the interactions are achieved by substituting alkyl groups for hydrogen atoms on the ammonium ion.

Fig. 1

Ionic Conductivity

Ionic Conductivity was determined from the low frequency touch down of arc in the Nyquist plot for all of these materials. As with the copolymers, two arcs were often observed on the heating runs, however, the resistance for both of these was very similar compared with the behavior observed in the copolymer systems. The

conductivity discussed here is obtained from the cooling runs where a single arc was usually observed. More details are presented in a later section. Fig. 2(a) presents the Arrhenius Plot of ionic conductivity for the (poly(N_{xyyy})$_{0.5}$$Na_{0.5}$[AMPS]) with three different tetraalkyl ammonium cations; the arrow indicates the T_g region of each ionomer. As noted in the trends in T_g discussed above, the polymer chain dynamics (ie. local segmental motions) are more facile in the N_{1444}^+ ionomer, and this seems to result in the highest conductivity amongst the ionomers investigated. In all cases the ionic conductivity follows an Arrhenius behavior, indicating a thermally activated conduction process that persists even below T_g. The activation energy in each case was 175(±2), 143(±11) and 120(±4) kJ/mol for the N_{1444}^+, N_{1222}^+ and N_{14111}^+ cations respectively. The higher activation energy for the bulkier cation is interesting and may reflect that, with increasingly lower temperatures in particular, the dynamics for this system are more difficult; however, with increasing temperature, the activation energy for diffusion can be overcome and the conductivity increases accordingly. Further evidence for this is shown from the NMR data discussed below.

The data shows that there is a significant measurable conductivity below T_g for all the ionomers, indicating decoupling of ionic conductivity from the local segmental motions that govern the T_g in these materials. In order to confirm this, we plot Log conductivity versus the reduced temperature T_g/T in Fig. 2(b). Sokolov's group[35] investigated the decoupling of ion transport from polymer segmental motion. In their work, they showed that, as temperature approached T_g the ionic conductivity approached $<10^{-12}$ S.cm^{-1}. This is typically what is expected when conductivity is coupled to the glass transition temperature of the polymer and is usually what one

observes for softer materials such polymer electrolytes based on PEO. In our case, the conductivity is up to three orders magnitude higher than this at T_g, therefore indicating an increasing decoupling of ion transport, especially for the N_{1444}^+ mixed cation system. From this representation of the data, we can directly observe that the ionic conduction does not solely rely on the segmental motions of the ionomer backbone that govern T_g, but is increasingly decoupled (higher conductivity at any reduced temperature) as the alkyl chains in the ammonium cation become more bulky. The idea of decoupling will be discussed in more detail when the different ratio of co-cations is discussed for the PAMPS homopolymer system.

The findings here correlate well with our previous work[19] in a sulfonate copolymer ionomer system, which showed that the ionic conduction was increasingly decoupled from T_g, particularly for compositions containing less than 50% Na. Thus it is again apparent that mixing two cations (ie. Na^+ and a quaternary ammonium cation) in an ionomer system leads to favorable behaviour for ion dynamics, in terms of decoupling of the ionic conductivity from the polymer segmental motions, in contrast to the findings when a single counterion is present (e.g. either only Na or only a bulky organic cation), as reported elsewhere[18, 31, 35]. The dependences of both conductivity and T_g on the chemical structure of the quaternary ammonium cation are shown in Fig. 3, which presents the measured conductivity at 423K together with the T_g for each ionomer.

Fig. 2

Fig. 3

NMR Characterisation

Solid-state NMR was used to characterize the ionomers and further study the dynamic behavior of the materials on a molecular level. The carbon spectra (Fig 4a) show the broad signals of the polymer backbone and narrow signals of the alkyl ammonium cations, indicating a higher mobility of the cations relative to the polymer chains. The signal assignment is as reported previously[19, 36]. The higher mobility of these species can also be seen in the narrow ^{15}N signals (Fig 4b) of the ammonium cations. The line width of the N_{1444} signal at -321 ppm of 47 Hz is slightly larger than the line width of N_{1222} (37 Hz) and $N_{14,111}$ (36 Hz). This indicates a slightly lower mobility of the more bulky N_{1444} compared to the other ammonium ions used and may be due to the larger, bulkier cation size in this case. The position of the ^{15}N chemical shift is also indicative of the changing electron density around the nitrogen center in these quaternary ammonium cations, which is dependent on the nature of the attached alkyl chains. As with the copolymer systems we recently reported, the sodium spectra (Fig 4c) of all samples are all quite similar and show a featureless, broad lineshape. Somewhat counter-intuitive to the T_g and conductivity data presented in Figure 3, the N_{1444} sample has a slightly broader lineshape. However, the data was measured at room temperature, and the activation energy from the conductivity data was shown to be significantly higher for the N_{1444} system, which could result in an overall lower mobility at lower temperatures. Further variable temperature studies are needed to better understand this behavior.

At this stage of development of these electrolytes, it can be ascertained qualitatively by NMR that the Na^+ ions are mobile. However, unlike lithium systems, the mobility of the ^{23}Na nuclei cannot currently be quantified via PFG-NMR

measurements. Measurements of transport number based on polarization experiments between two electrodes reversible to Na^+ will be considered in the future, but this is beyond the scope of this paper which focuses on assessing the conductivity parameters and their dependence on T_g.

Fig. 4

2. Effect of sodium content in the homopolymer of (Poly(N_{1222})$_z$Na$_{1-z}$[AMPS])

In our previous work, we reported the effect of Na content in a copolymer of poly([N_{1222}][AMPS]-co-Na[VS]) ionomers. The data show that the conductivity is increasingly decoupled from the T_g of the ionomer systems as the Na^+ concentration decreased. In this section we discuss the effect of Na content in a PAMPS homopolymer with different ratios of N_{1222} and Na^+ counterions (Poly(N_{1222})$_z$Na$_{1-z}$[AMPS]) to compare the differences between homopolymer and copolymer ionomer systems.

Thermal Properties

Fig. 5 shows the DSC thermograms of ionomers with different Na contents. As expected, the T_g increases (indicating segmental motion within the ionomers is reduced) with a decreasing fraction of the bulky cation, since the interchain interactions are stronger with higher Na^+ content due to enhanced electrostatic attractions between chain segments. This data is in contrast with copolymer ionomers system, where the T_g did not vary significantly as the Na content went from 10 to 50%. The glass transitions of the homopolymer systems presented here are also not as broad as in the case of the copolymer materials[19]. The broadness of

the glass transition has been calculated from the difference between onset and endpoint of each DSC thermogram. For example, the width of 20% Na copolymer system is 28 ^{o}C while in the homopolymer system, with the same Na content, it is only 13 ^{o}C. This is less than half the value for the copolymer systems, which may reflect a more homogenous material in this case. This behavior will be further discussed in the ionic conductivity and morphology section below.

Fig. 5

Ionic Conductivity

The Nyquist plot for the ionomer containing 10% Na^+ (Poly(N_{1222})$_{0.9}$Na$_{0.1}$[AMPS]) at 373 K (below T_g) and at 403 K (above T_g) are presented in Fig. S1. Below T_g, two semicircles can be observed, in addition to the low frequency electrode polarization spike, indicating two conduction processes might be present. In order to calculate the total conductivity of the ionomers, the conductivity data has been fitted with a series circuit as depicted in Fig. S2. Example fitting data has also been included in a Table (SI) to illustrate the parameters obtained and the goodness of fit. Similar observations were encountered in the copolymer system discussed in our previous work[19], where two distinguishable semicircles appeared in the Nyquist plot below the T_g of the samples. However, in the homopolymer system, the two semicircles are not as clearly separated, which might again reflect greater homogeneity. However, some degree of inhomogeneity can still be detected at the microscopic level as will be discussed further below. Fig. 6 presents the Arrhenius plots of each of the ionomers with various compositions, from 0 to 100% Na, with arrows showing the T_g region in each case. From this data, it can be seen that the 50% and 100% Na samples show very low conductivity, consistent with a high T_g and coupled ion

motion. The strong associations of Na^+ to the sulfonate anion on the ionomer backbone and the interchain electrostatic crosslinking that results, leads to a reduction of the segmental motion of the ionomers as previously reported elsewhere.[19, 31, 35]

On the other hand, below 20% Na^+, the ionic conductivity shows curvature consistent with Vogel-Tamman-Fulcher (VTF) behavior[7, 37]. VTF behaviour suggests that migration of the ions in the ionomer systems is similar to ionic conduction observed in the case of a liquid. If the ionic conductivity follows VTF behaviour, the plot of log conductivity versus $1000/(T-T_o)$ should present a straight line. In order to confirm this, we show log conductivity versus inverse temperature of $(T-T_o)$, where T_o was taken from the fitted VTF parameter value as depicted in Fig. S3. A straight line (with a regression coefficient of 0.999) can be observed from this plot, indicating the ionomers containing less than 20% Na^+ indeed follow VTF behaviour over this temperature range. The values of the fitted VTF parameters are summarized in Table 1.

Table1

Furthermore, a measureable conductivity can be observed below T_g for all samples, which indicates the ionic conductivity is again increasingly decoupled from the segmental motion of the polymers. Fig. 7 normalizes the temperature by the DSC T_g, showing that the segmental motion of the ionomer backbone is not the sole source of improvement in ionic conductivity. A remarkable finding is that the conductivity at fixed T_g/T shows 10% Na^+ possesses the highest ionic conductivity among all the systems studied here. This is consistent with the behavior we previously observed in

the copolymer ionomers where 10% Na^+ shows the highest conductivity of all the samples investigated[19]. Hence it appears that incorporation of two cations leads to favorable properties for conductivity in these materials (both copolymer and homopolymer ionomer systems), especially for lower Na^+ concentrations. The conduction process involved is probably a combination of the quaternary ammonium cation motion and Na^+ motion. The idea behind this family of electrolytes is that, by partial replacement of Na^+ by NR_4^+, this increases the number of energetically equivalent SO_3^- sites available for each sodium. This contributes an entropic component to the Na-polymer dissociation equilibrium, thus facilitating hopping type motions, even in a glassy material. This is in line with conduction models in inorganic glass and ceramic electrolytes.

As shown earlier, the conductivity at T_g is significantly greater than 10^{-12} $S.cm^{-1}$, the value that would be expected if conductivity is coupled to T_g. The systems with a lower Na ion concentration appear to be extensively decoupled in the case where N_{1222}^+ cation replaces the Na cation. Interestingly, the previous work by Wang et. al.,[35] suggests that, even when the ionic conductivity is coupled to the T_g of the polymer electrolyte, there is still extensive decoupling of ion transport from local segmental polymer motions as measured by dielectric spectroscopy, especially those that are more rigid. This was evidenced from a comparison of a structural relaxation time that was extracted from dielectric relaxation and the ionic conductivity. The authors suggest that this relaxation time is in fact related to the local segmental motions of the polymer and that T_g is not the appropriate parameter to consider for decoupling of ion dynamics from polymer segmental motions, since in their case, decoupling from T_g was not generally observed. Nevertheless, the parameter

extracted to define local segmental motion in their case certainly indicated that some systems had a significant degree of decoupling of the conductivity, and this was correlated with the polymer electrolyte's fragility[35, 38, 39]. They postulated that in polymers that possesses high fragility, ions can freely move throughout the loose structure which results from frustrated packing, even if the structure has overall very slow segmental relaxation. Conversely, greater flexibility produces a more dense structure (i.e. well packed polymer chains), hence less fragility and ion mobility only occurs when polymer segments are able to move. They also suggested that condensed structures (i.e least fragile) can form from well-packed, flexible chains and will show almost Arrhenius temperature dependence of the segmental dynamics, while strongly non-Arrhenius temperature variations can be exhibited by the frustrated packing of rigid chains from forming a loose structure (i.e very fragile systems). Thus it appears that the incorporation of a larger quaternary ammonium cation such as N_{1222}^{+} with increasing concentration, in the present materials, leads to a looser packing (increased free volume) of the polymer chains and hence higher fragility despite T_g not being significantly affected. Thus the enhanced decoupling observed in the present systems may result from such an increase in free volume, which supports ion hopping.

Fig. 6

Fig. 7

3. The effect of plasticizer in the poly([N_{1222}][AMPS]-Na) ionomers

The ionic conductivity of the 50% Na^{+} ionomer system (Poly$(N_{1222})_{0.5}Na_{0.5}$[AMPS]) is very low, consistent with a high glass transition temperature as discussed above. However, when the conductivity is scaled by T_g, this system also shows some

decoupling from the backbone dynamics that determine T_g. An addition of 10 wt.% of plasticizer to the copolymer ionomer system showed that the ionic conductivity improved by three orders or magnitude[19]. We therefore also investigated the incorporation of plasticizer for the homopolymer system to observe if higher ionic conductivities can be obtained in this system. Fig. 8 (a) and (b) present the conductivity of plasticized ionomers in Arrhenius format and scaled with respect to T_g respectively. The T_g of the plasticized ionomers (arrows in the Arrhenius plot) does not change significantly compared to the unplasticized material, however, the ionic conductivity increased dramatically, up to three orders of magnitude, when the IL is incorporated as a plasticizer, and by one and a half orders when tetraglyme (G4) is added. Furthermore it appears that the ionic conductivity in these plasticized systems is even more strongly decoupled from the bulk T_g of the materials. The effect of IL plasticizer on the 10% Na^+ ionomer system was also investigated and in this case the ionic conductivity increased by nearly a factor of 100, as can be seen in Fig. 8. This additional increase may be at least in part due to the presence of additional ions from the IL.

Fig. 8

Fig. 9

Morphology

As discussed in the thermal properties and ionic conductivity sections, the broad glass transition observed and the presence of two semicircles in the Nyquist plot may reflect heterogeneity or phase separation within these ionomers. In contrast to the copolymer systems, the T_g is not as broad and the two semicircle also are not as clearly separated. Interestingly, whereas phase separation was clearly visible in the

copolymer systems using optical microscopy, this is not the case for the homopolymer systems discussed in the present work; thus the phase separation cannot be detected by optical microscopy, as seen in Fig. S4. However, to investigate whether phase separation might have occurred at a smaller length scale, or even at a nano level (given that we do observe two semicircle in the Nyquist plot), we performed micro- Raman Spectroscopy. This provides sub-micron spatial resolution to precisely choose the area of interest in which to carry out chemical analysis. The chemical mapping of polymer blends or composites, based on their characteristic Raman peaks, can be used to probe the domains of phase separated polymer blends with phase domain sizes as small as ~200nm[40].

Before mapping, the ionomer samples were positioned in the laser focus using a video camera and white-light illumination. A suitable region was chosen that appeared relatively flat. Preliminary studies on the spectra of the three ionomers (0%, 50% and 100% Na^+) showed that there was very useful information in the 1500 – 300 cm^{-1} spectral regions (Fig. S5); therefore, spectra were only collected in this region to reduce the measurement time. Fig. 10 (a) presents the fine Raman map of ionomers from 1100 – 600 cm^{-1}. The presence of bright and dark regions can clearly be seen, indicating phase separation might have occurred in this ionomer.

The phase separation observed in Raman imaging results was also verified by SEM observation of the (Poly$(N_{1222})_{0.5}Na_{0.5}$[AMPS]) sample, as shown in Fig. 10 (b). In this case we observe the presence of dark and bright areas, and the bright areas represent a 'network' that correlates well with the bright regions from the Raman imaging results.

Fig. 10

CONCLUSIONS

Notwithstanding the strong decoupling behavior, the ionic conductivity of the ionomers investigated in this work is still too low for them to be considered for practical devices. In part this is due to the relatively high T_g values but predominantly, also to the strong ionic interactions between the sodium and the conduction sites available for the sodium ions to 'hop' between. Introduction of plasticizer into the ionomers significantly increased the ionic conductivity, by up to three orders magnitude. In this paper, we also showed that a bulky ionic quaternary ammonium cation is necessary in order to reduce the electrostatic interchain interactions. It is therefore possible to synthesize copolymer ionomers with a bulky quartenary ammonium counterion, while preserving the decoupling properties. If these two factors are adequately addressed, such ionomers would be promising candidates for realizing single ion conduction with high ionic conductivity in solid-state electrolytes.

ACKNOWLEDGEMENTS

The authors are grateful to the Australian Research Council for funding via DP130101652 and under the Laureate Fellowship schemes (MF and DRM). We also acknowledge the ARC for support of the NMR facility through the grant LE110100141

REFERENCES

1. Noor, S. A. M.; Ahmad, A.; Talib, I. A.; Rahman, M. Y. A. *Ionics* **2010,** *16*, 161-170.
2. Morita, M.; Shirai, T.; Yoshimoto, N.; Ishikawa, M. *J. Power Sources* **2005,** *139*, 351-355.
3. Mohd Noor, S. A.; Howlett, P. C.; Macfarlane, D. R.; Forsyth, M. *Electrochim. Acta* **2013,** *114*, 766-771.
4. Kumar, D.; Hashmi, S. A. *Solid State Ionics* **2010,** *181*, 416-423.
5. Gayet, F.; Viau, L.; Leroux, F.; Monge, S.; Robin, J. J.; Vioux, A. *J. Mater. Chem.* **2010,** *20*, 9456-9462.
6. Fenton, D. E.; Parker, J. M.; Wright, P. V. *Polymer* **1973,** *14*, 589.
7. Gray, F. M., *Solid polymer electrolytes : fundamentals and technological applications*. New York, NY : VCH: New York, NY, 1991.
8. Noor, S. A. M.; Ahmad, A.; Rahman, M. Y. A.; Talib, I. A. *J. Appl. Polym. Sci.* **2009,** *113*, 855-859.
9. Ueno, K.; Hata, K.; Katakabe, T.; Kondoh, M.; Watanabe, M. *J. Phys. Chem. B* **2008,** *112*, 9013-9019.
10. Tiyapiboonchaiya, C.; Pringle, J. M.; MacFarlane, D. R.; Forsyth, M.; Sun, J. *Macromol. Chem. Phys.* **2003,** *204*, 2147-2154.
11. Roach, D. J.; Dou, S.; Colby, R. H.; Mueller, K. T. *J. Chem. Phys.* **2012,** *136*.
12. Travas-Sejdic, J.; Steiner, R.; Desilvestro, J.; Pickering, P. *Electrochim. Acta* **2001,** *46*, 1461-1466.
13. Capuano, F.; Croce, F.; Scrosati, B. *J. Electrochem. Soc.* **1991,** *138*, 1918-1922.
14. Appetecchi, G. B.; Zane, D.; Scrosati, B. *J. Electrochem. Soc.* **2004,** *151*, A1369-A1374.
15. Evans, J.; Vincent, C. A.; Bruce, P. G. *Polymer* **1987,** *28*, 2324-2328.
16. Watanabe, M.; Nishimoto, A. *Solid State Ionics* **1995,** *79*, 306-312.
17. Tudryn, G. J.; O'Reilly, M. V.; Dou, S.; King, D. R.; Winey, K. I.; Runt, J.; Colby, R. H. *Macromolecules* **2012,** *45*, 3962-3973.
18. Wang, W.; Tudryn, G. J.; Colby, R. H.; Winey, K. I. *J. Am. Chem. Soc.* **2011,** *133*, 10826-10831.
19. Mohd Noor, S. A.; Gunzelmann, D.; Sun, J.; MacFarlane, D. R.; Forsyth, M. *Journal of Materials Chemistry A* **2014,** *2*, 365-374.
20. Kobayashi, N.; Uchiyama, M.; Tsuchida, E. *Solid State Ionics* **1985,** *17*, 307-311.
21. Zheng, S.-s.; Liu, Q.-g.; Yang, L.-l. *Polymer* **1994,** *35*, 3740-3744.
22. Ünal, H. I.; Yilmaz, H. *J. Appl. Polym. Sci.* **2002,** *86*, 1106-1112.
23. Annala, M.; Lipponen, S.; Kallio, T.; Seppälä, J. *J. Appl. Polym. Sci.* **2012,** *124*, 1511-1519.
24. Santiago, A. A.; Vargas, J.; Cruz-Gómez, J.; Tlenkopatchev, M. A.; Gaviño, R.; López-González, M.; Riande, E. *Polymer (United Kingdom)* **2011,** *52*, 4208-4220.

25. Byrne, N.; Howlett, P. C.; MacFarlane, D. R.; Forsyth, M. *Adv. Mater. (Weinheim, Ger.)* **2005,** *17*, 2497-2501.
26. Park, M. J.; Kim, S. Y. *J. Polym. Sci., Part B: Polym. Phys.* **2013,** *51*, 481-493.
27. Kar, M.; Winther-Jensen, B.; Forsyth, M.; MacFarlane, D. R. *Phys. Chem. Chem. Phys.* **2013,** *15*, 7191-7197.
28. Tang, S.; Baker, G. A.; Zhao, H. *Chem. Soc. Rev.* **2012,** *41*, 4030-4066.
29. Tamura, T.; Yoshida, K.; Hachida, T.; Tsuchiya, M.; Nakamura, M.; Kazue, Y.; Tachikawa, N.; Dokko, K.; Watanabe, M. *Chem. Lett.* **2010,** *39*, 753-755.
30. Eisenberg, A.; Kim, J.-S., *Introduction to ionomers*. Wiley Inter-Science: New York, 1998.
31. Tudryn, G. J.; Liu, W.; Wang, S. W.; Colby, R. H. *Macromolecules* **2011,** *44*, 3572-3582.
32. Lefelar, J. A.; Weiss, R. A. *Macromolecules* **1984,** *17*, 1145-1148.
33. Grady, B. P.; Moore, R. B. *Macromolecules* **1996,** *29*, 1685-1690.
34. Weiss, R. A.; Agarwal, P. K.; Lundberg, R. D. *J. Appl. Polym. Sci.* **1984,** *29*, 2719-2734.
35. Wang, Y.; Agapov, A. L.; Fan, F.; Hong, K.; Yu, X.; Mays, J.; Sokolov, A. P. *Phys. Rev. Lett.* **2012,** *108*.
36. Shestakova, P.; Willem, R.; Vassileva, E. *Chemistry - A European Journal* **2011,** *17*, 14867-14877.
37. Smedley, S. I., *The interpretation of ionic conductivity in liquids*. New York : Plenum Press Wellington, New Zealand, 1980; p 195.
38. Agapov, A. L.; Sokolov, A. P. *Macromolecules* **2011,** *44*, 4410-4414.
39. Ediger, M. D.; Harrowell, P.; Yu, L. *J. Chem. Phys.* **2008,** *128*.
40. Kumar, C. S. S. R., *Raman spectroscopy for nanomaterials characterization*. Berlin ; New York : Springer: Baton Rouge, LA, USA, 2012.

List of Figures

Scheme 1 (a) Schematic preparation of (poly(N_{1222})$_z$$Na_{1-z}$[AMPS]) ionomers (b) cationic counterion structures: triethylmethylammonium (N_{1222}^+), tributylmethylammonium (N_{1444}^+) and trimethyltetradecylammonium ($N_{14,111}^+$)

Fig. 1 DSC thermograms of (Poly(N_{xyyy})$_{0.5}$$Na_{0.5}$[AMPS]) ionomers with different types of quaternary cation where x and y reflect different length alkyl chains on the Nitrogen atom.

Fig. 2 (a) Arrhenius conductivity plot of (Poly(N_{xyyy})$_{0.5}$$Na_{0.5}$[AMPS]) ionomers with different types of quaternary ammonium cation. The arrows represent T_g in each system (b) ionic conductivity of the ionomers as a function of quaternary ammonium cation with the inverse temperature normalized by T_g for each polymer

Fig. 3 Ionic conductivity at 423K and the glass transition temperature (T_g) of (Poly(N_{xyyy})$_{0.5}$$Na_{0.5}$[AMPS]) ionomers as a function of tetraalkylammonium cation

Fig. 4 CPMAS spectra of the ionomers containing different ammonium ions. (a) ^{13}C (b) ^{15}N (c) ^{23}Na. Spectra were recorded at room temperature and 10 kHz magic angle spinning (MAS).

Fig. 5 DSC thermograms of (Poly(N_{1222})$_z$$Na_{1-z}$[AMPS]) ionomers with different mol% of Na

Fig. 6 Arrhenius conductivity plot of (Poly(N_{1222})$_z$$Na_{1-z}$[AMPS]) ionomers with various mol% of Na. The arrows indicate the T_g for each system.

Fig. 7 Ionic conductivity of the ionomers as a function of Na^+ concentrations and temperature normalized by T_g

Fig. 8 (a) Arrhenius conductivity plot of (Poly(N_{1222})$_{0.5}$$Na_{0.5}$[AMPS]) ionomers with 10 wt.% IL and tetraglyme (b) Ionic conductivity of the ionomers as a function of plasticizer and temperature normalized by T_g

Fig. 9 Arrhenius conductivity plot of (Poly(N_{1222})$_{0.9}$$Na_{0.1}$[AMPS]) ionomers with 10 wt.% IL

Fig. 10 (a) fine map of ionomers from 1100 – 600 cm^{-1} (b) SEM images of the 50% Na^+ ionomers

List of Table

Table 1 VTF ionic conductivity parameters for (Poly$(N_{1222})_zNa_{1-z}$[AMPS])

Figures

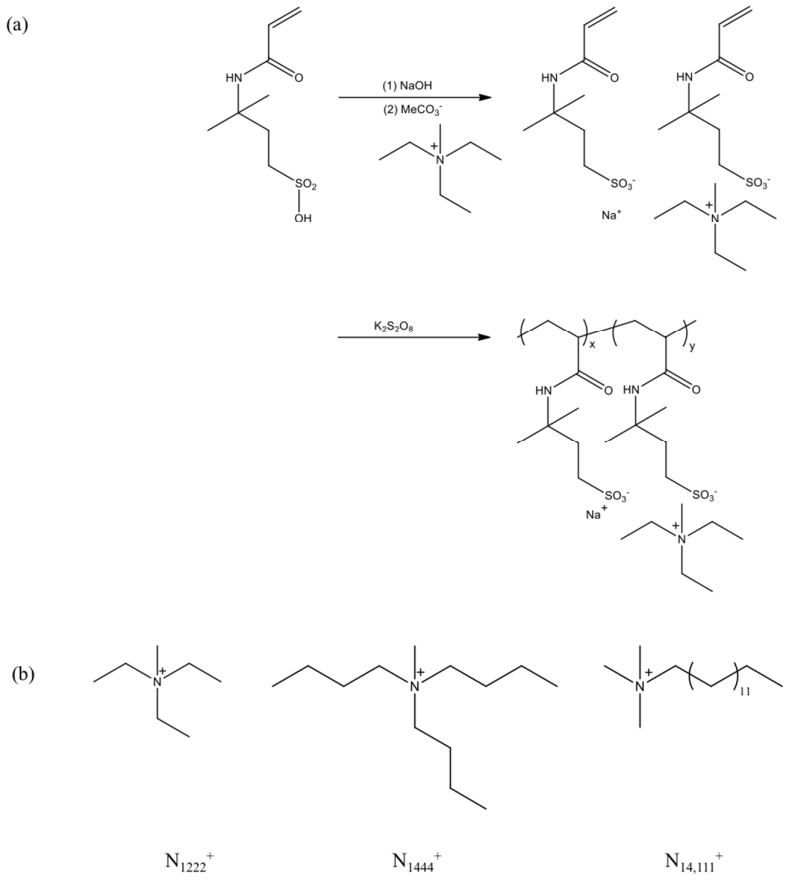

Scheme 1 (a) Schematic preparation of (poly$(N_{1222})_zNa_{1-z}$[AMPS])**.** ionomers (b) cationic counterion structures: triethylmethylammonium (N_{1222}^+), tributylmethylammonium (N_{1444}^+) and trimethyltetradecylammonium ($N_{14,111}^+$)

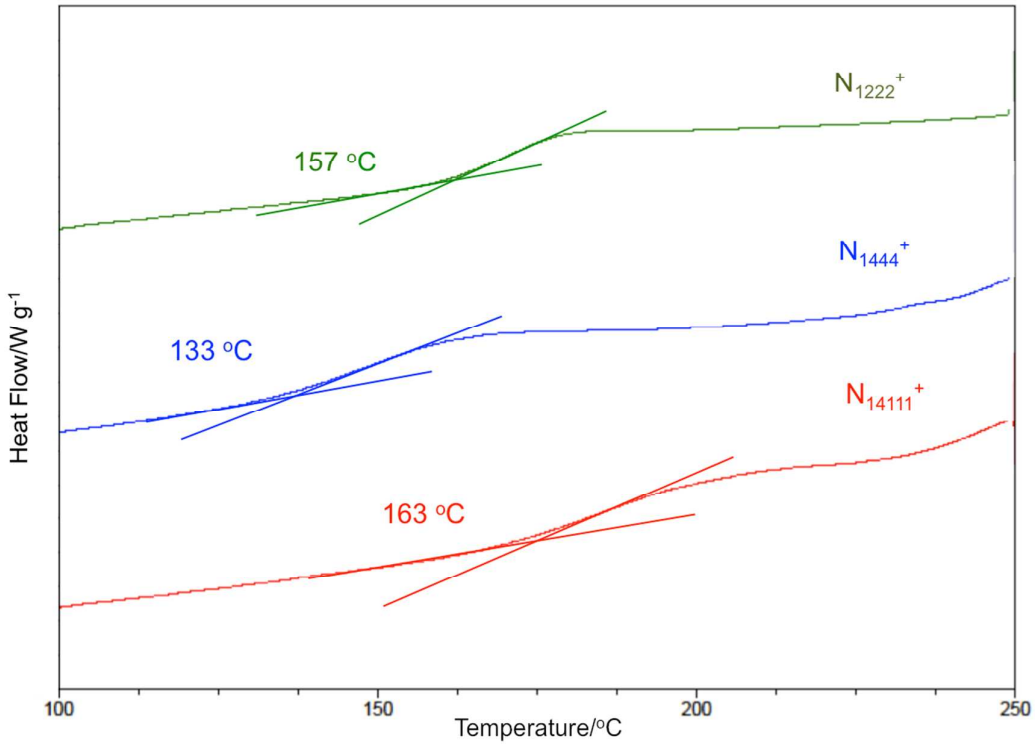

Fig. 1 DSC thermograms of (Poly(N_{xyyy})$_{0.5}$Na$_{0.5}$[AMPS]) ionomers with different types of quaternary cation where x and y reflect different length alkyl chains on the Nitrogen atom.

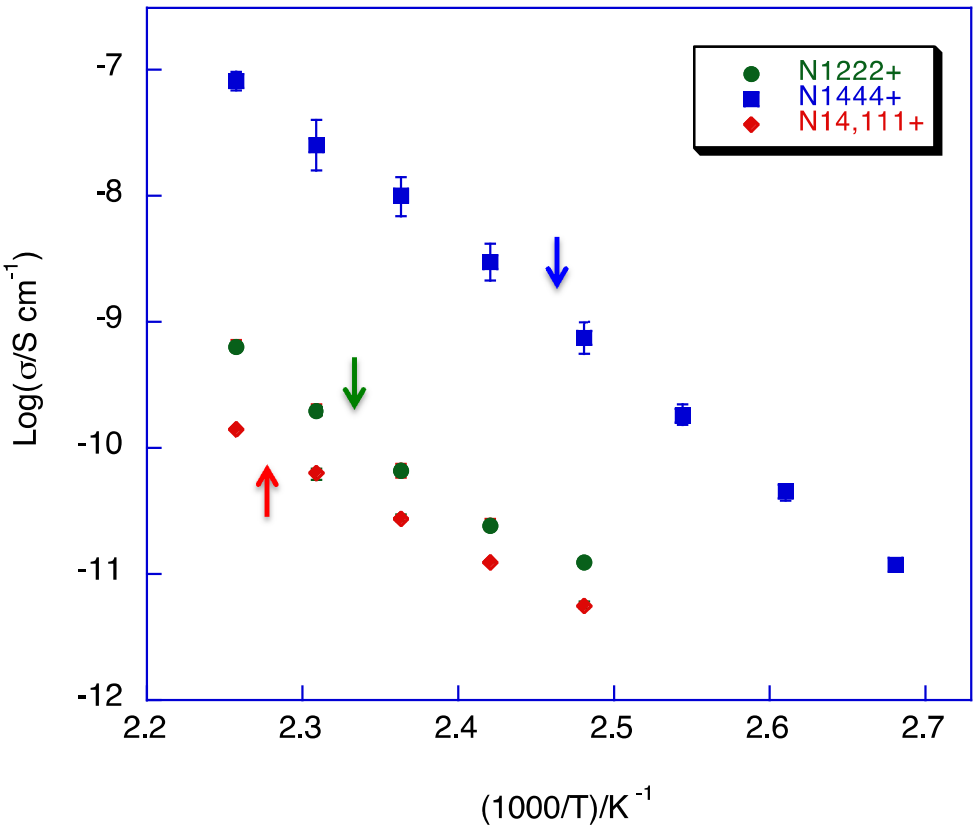

(a)

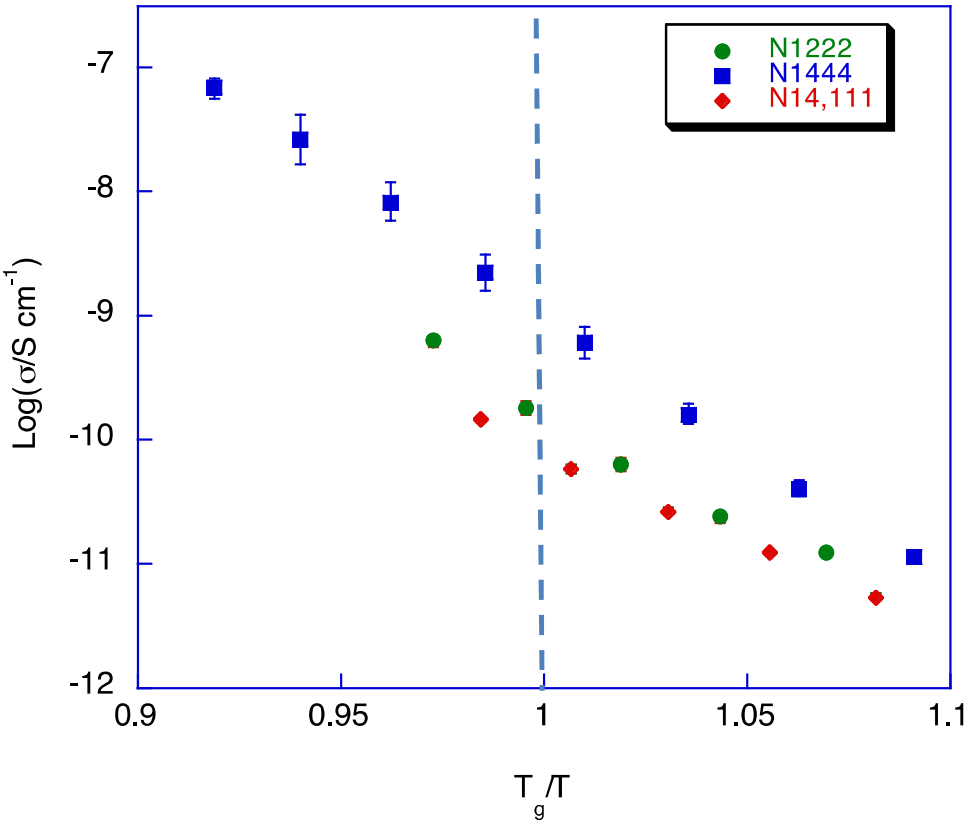

(b)

Fig. 2 (a) Arrhenius conductivity plot of $(Poly(N_{xyyy})_{0.5}Na_{0.5}[AMPS])$ ionomers with different types of quaternary ammonium cation. The arrows represent T_g in each system (b) ionic conductivity of the ionomers as a function of quaternary ammonium cation with the inverse temperature normalized by T_g for each polymer

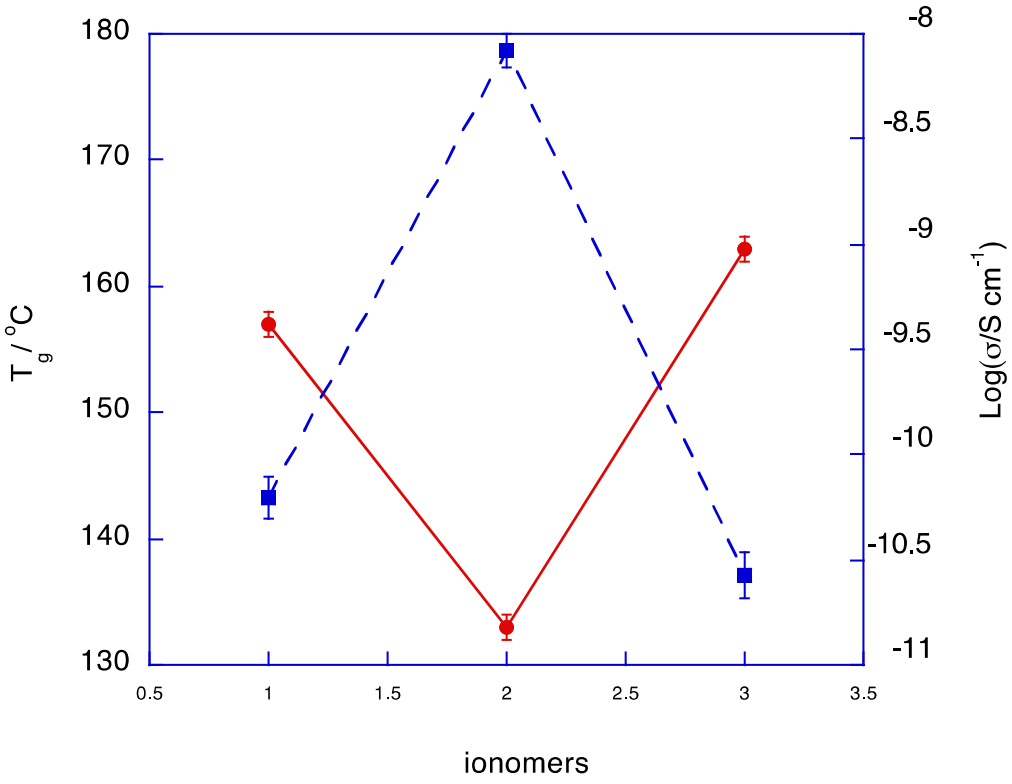

Fig. 3 Ionic conductivity at 423K and the glass transition temperature (T_g) of (Poly(N_{xyyy})$_{0.5}$Na$_{0.5}$[AMPS]) ionomers as a function of tetraalkylammonium cation

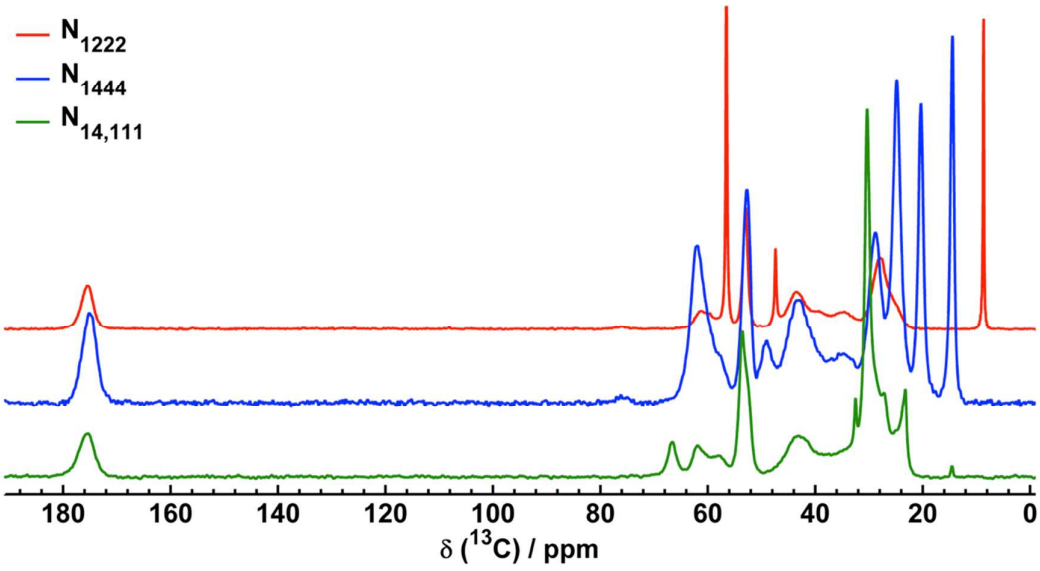

(a)

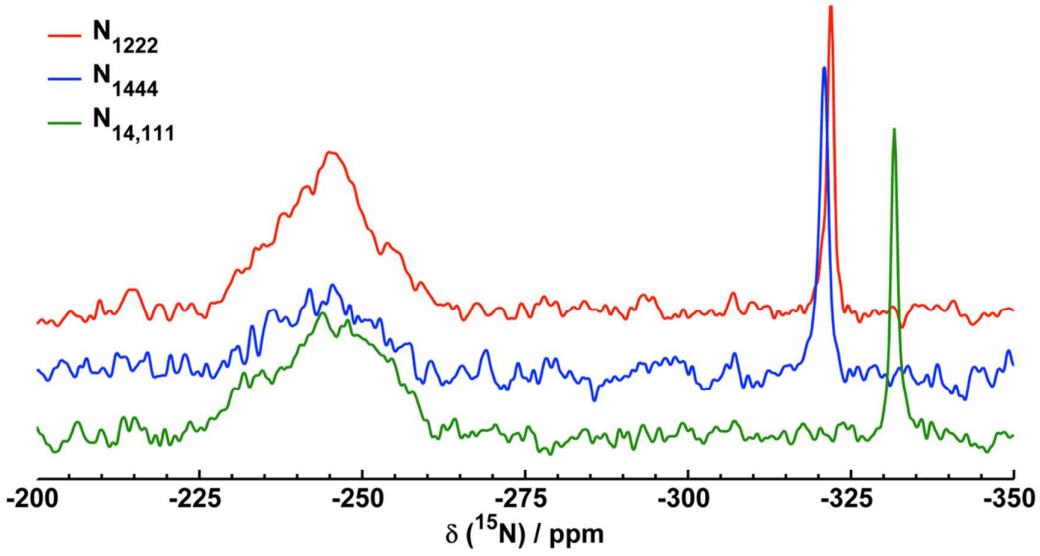

(b)

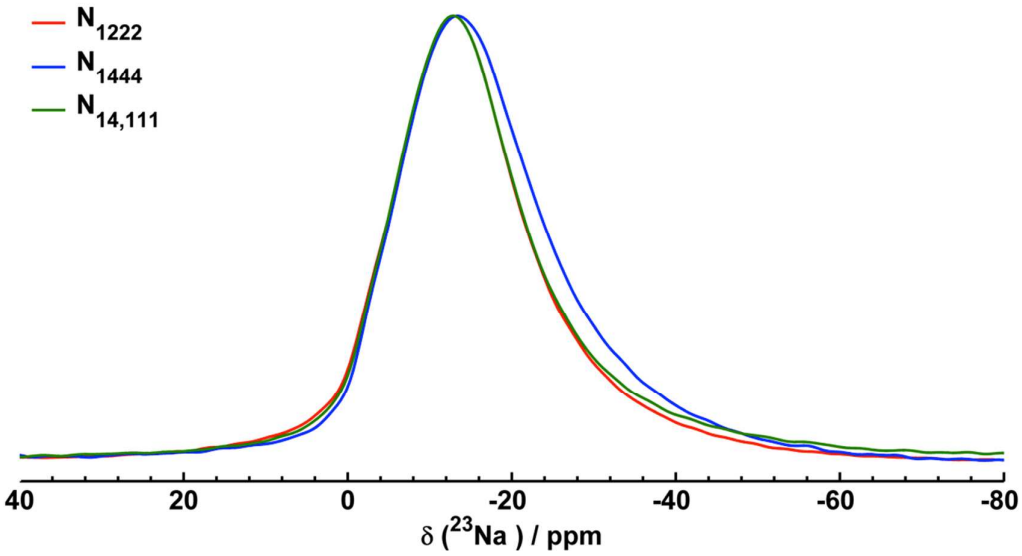

(c)

Fig. 4 CPMAS spectra of the ionomers containing different ammonium ions. (a) ^{13}C (b) ^{15}N (c) ^{23}Na. Spectra were recorded at room temperature and 10 kHz magic angle spinning (MAS).

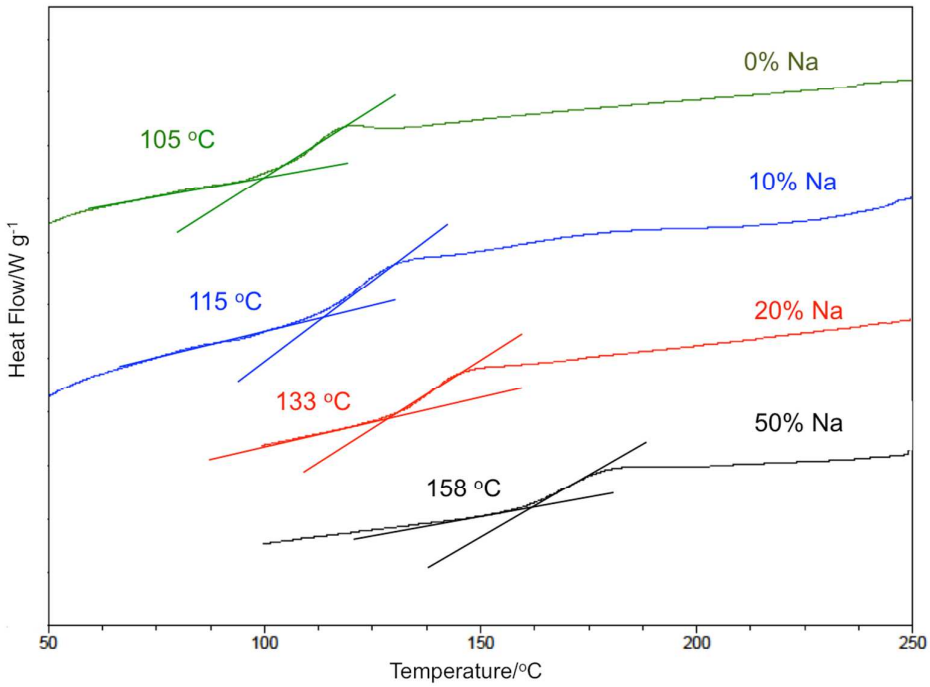

Fig. 5 DSC thermograms of (Poly(N_{1222})$_z$$Na_{1-z}$[AMPS]) ionomers with different mol% of Na

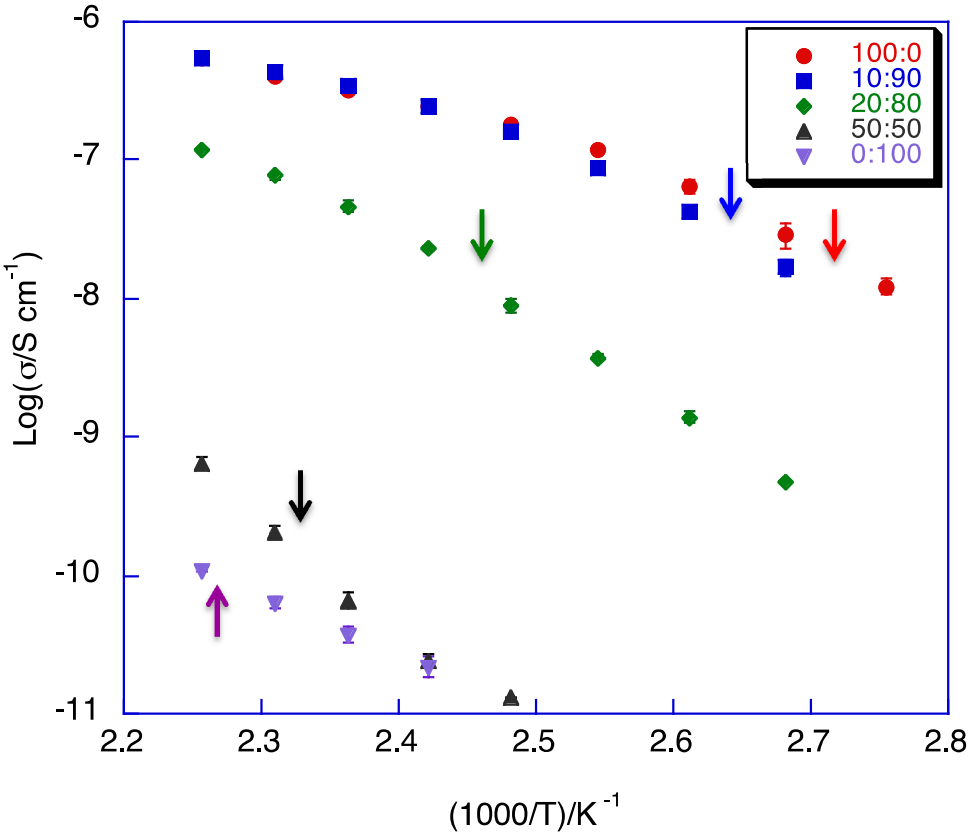

Fig. 6 Arrhenius conductivity plot of (Poly(N_{1222})$_z$$Na_{1-z}$[AMPS]) ionomers with various mol% of Na. The arrows indicate the T_g for each system.

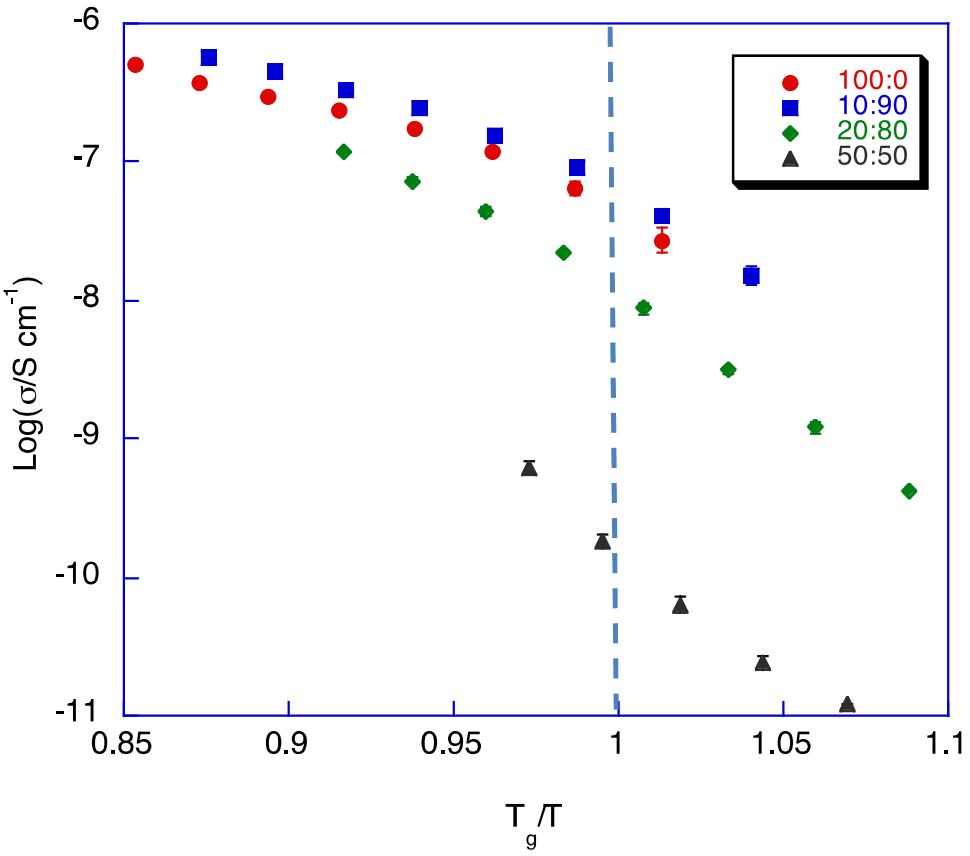

Fig. 7 Ionic conductivity of the ionomers as a function of Na^+ concentrations and temperature normalized by T_g

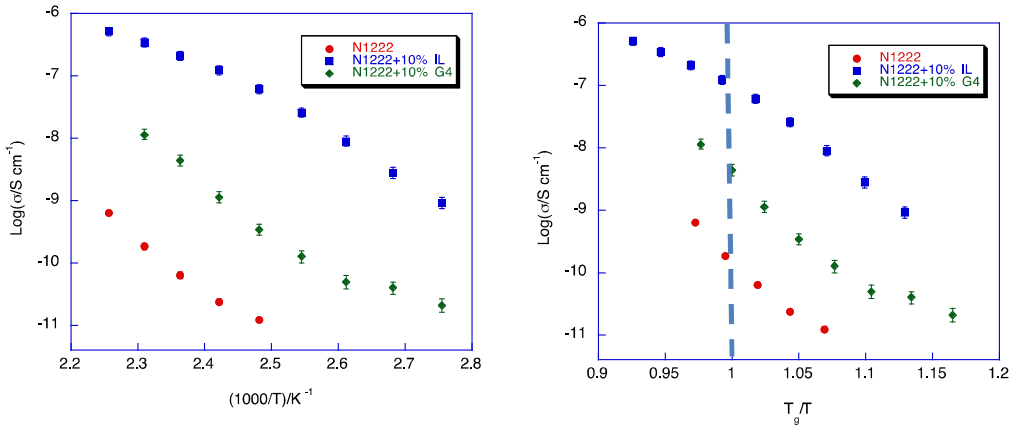

Fig. 8 (a) Arrhenius conductivity plot of (Poly(N_{1222})$_{0.5}$$Na_{0.5}$[AMPS]) ionomers with 10 wt.% IL and tetraglyme (b) Ionic conductivity of the ionomers as a function of plasticizer and temperature normalized by T_g

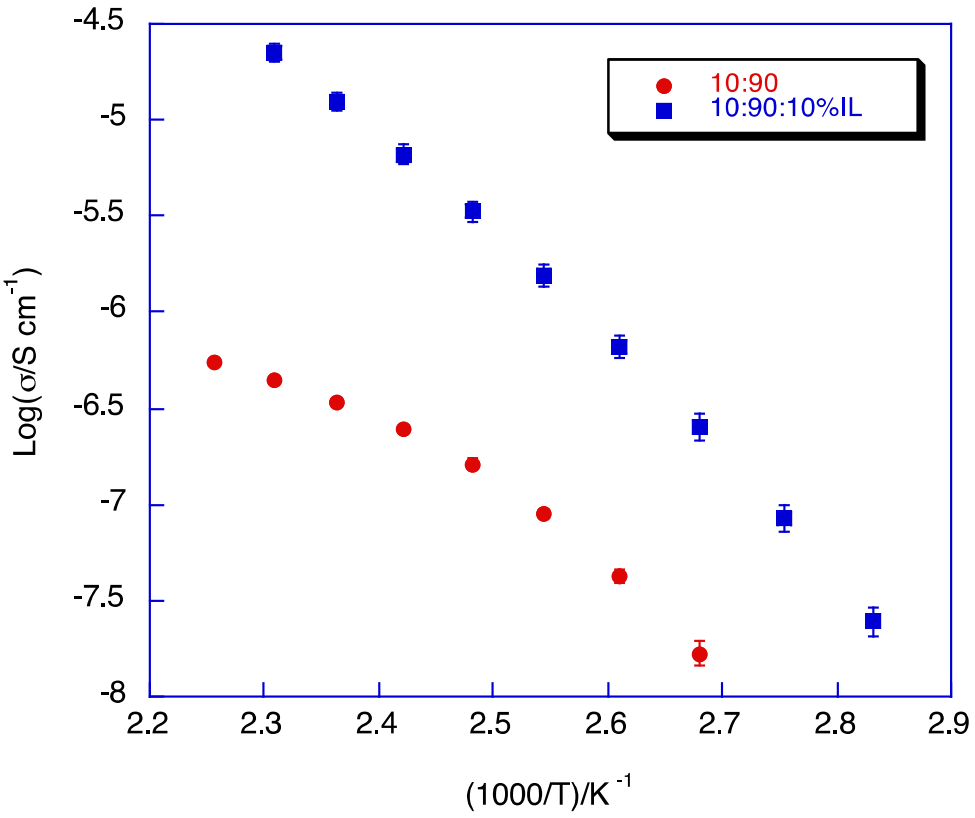

Fig. 9 Arrhenius conductivity plot of (Poly(N_{1222})$_{0.9}$$Na_{0.1}$[AMPS]) ionomers with 10 wt.% IL

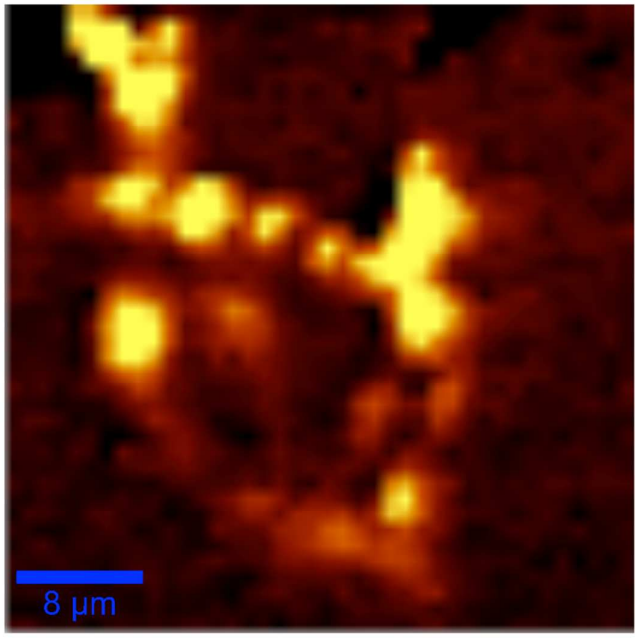

(a)

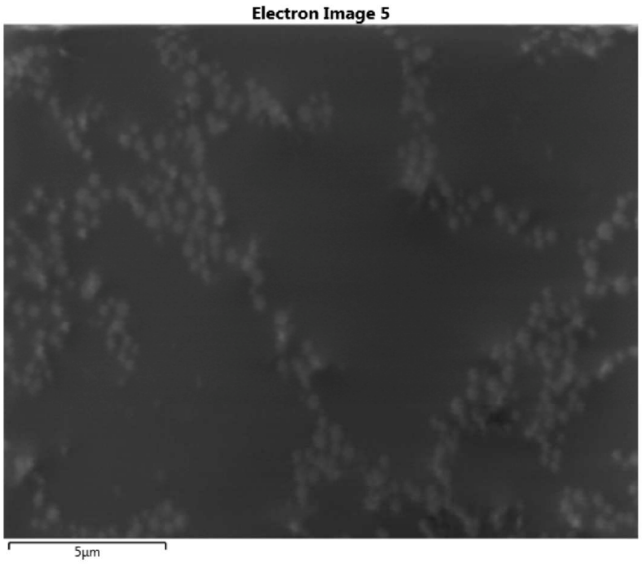

(b)

Fig. 10 (a) fine map of ionomers from 1100 – 600 cm^{-1} (b) SEM images of the 50% Na^{+} ionomers

Table

Table 1 VTF ionic conductivity parameters for (Poly(N_{1222})$_z$$Na_{1-z}$[AMPS])

Na^+ (mol%)	Log σ_o/S cm^{-1}	B/K	T_o/K	R
0	-5.2±0.1	-140±22	311±6	0.999
10	-5.2±0.1	-132±9	324±2	0.999
20	-2.4±0.9	-912±317	245±27	0.999